Pergamon

S0967–0637(96)00009–X

Deep-Sea Research I, Vol. 43, No. 2, pp. 117–138, 1996

0967–0637/96 $15.00 + 0.00

Seasonal variations of sea-surface salinity and temperature in the tropical Indian Ocean

JEAN-RENE DONGUY* and GARY MEYERS†

(*Received* 7 *February* 1994; *in revised form* 9 *November* 1995; *accepted* 27 *November* 1995)

Abstract—Measurements of sea-surface temperature and sea-surface salinity obtained from ships-of-opportunity are used to map the fields in the tropical Indian Ocean. The seasonal variation is described in detail along the six shipping tracks that have the best data coverage: Gulf of Aden to La Reunion island, Persian Gulf to Cape Town, Gulf of Aden to east Africa, Gulf of Aden to Indonesia, Sri Lanka to Torres Strait through Malacca Strait, and along the west coast of Australia. Seasonal variation with large amplitude is found in an extensive area in the western Indian Ocean. In the eastern Indian Ocean, seasonal variation is small, except where it is linked to local features such as coastal upwelling, local wind or rainfall–runoff. Water masses, defined from the surface T–S diagram, are related to winds and currents or are formed locally. The movement of these water masses is linked to currents driven by the monsoon circulation. Copyright © 1996 Elsevier Science Ltd.

1 INTRODUCTION

The long-term mean field of sea-surface salinity (SSS) has been described in atlases; however, its variability is poorly known at the oceanic scale. Recently, there has been a surge of interest in the large-scale patterns of SSS for several reasons. Salinity is the result of the exchange of water at the atmosphere–ocean interface and consequently is a sensitive index of the global climate system. It also affects the storage of heat in the surface layer, at least in the western Pacific (Lukas, 1989), and must be included in the ENSO scenario. Finally, it is a parameter in the dynamic calculation of geostrophic currents from XBT profiles and in three-dimensional ocean models.

With the help of officers and crews of ships-of-opportunity, ORSTOM has collected a unique set of routine surface data, including sea-surface temperature (SST) and SSS, over three oceans: from 1969 to the present in the tropical Pacific Ocean; from 1977 to the present in the tropical Atlantic Ocean; from 1966 to 1967 and from 1977 to the present in the tropical Indian Ocean. From this worldwide data set, recent studies have documented SSS and SST in the tropical Pacific Ocean (Delcroix and Henin, 1989, 1991) and in the tropical Atlantic Ocean (Dessier and Donguy, 1994). In the tropical Indian Ocean, earlier studies of the western part used the 1966–1967 data (Donguy, 1970, 1974, 1975). Also worth mentioning are the bi-monthly SSS and monthly SST charts in the International Indian Ocean Expedition Atlas by Wyrtki (1971) and the monthly SST charts by Sadler *et al.* (1987) based on the Comprehensive Ocean–Atmospheric Data Set (COADS) for the period 1850–1979.

*Centre ORSTOM de Brest, BP 70, 29280 Plouzane, France.
†CSIRO Division of Oceanography, GPO Box 1538, Hobart, Tasmania 7001, Australia.

The ORSTOM sea-surface data set was merged with all the available additional surface data (and particularly CSIRO data) to produce a reliable climatology. There are sufficient data to reliably document the seasonal variations of SSS in some regions, but irregularities in space and time do not allow as yet documentation of the large-scale interannual variations.

This article is organised as follows: Section 2 presents the surface data set, data processing and expected errors; Section 3 presents the seasonal cycles of SSS and SST along shipping tracks; Section 4 presents a classification of water masses from a *T–S* diagram; Section 5 presents bi-monthly charts of SSS, and their connection with the climate system is discussed; and Section 6 presents a comparison with earlier studies.

2 DATA AND DATA PROCESSING

Surface data in the tropical Indian Ocean were compiled for the region from 30°N to 40°S and from 30°E to 140°E (Fig. 1). The ORSTOM data set was collected by ships-of-opportunity operating from Nosy Be (Madagascar) from 1966 to 1968, from Noumea (New Caledonia) from 1969 to 1992, and from Marseille and Le Havre (France) from 1977 to 1992. Most of the data were collected along the merchant shipping tracks (Fig. 1). For the SSS measurements, water was sampled at the sea surface, four times a day, with a bucket, and later analysed on shore by a laboratory salinometer. The SST measurements were obtained from a thermometer fitted inside the bucket or from a thermograph. A total of 44,573 surface observations were available in the ORSTOM archive. The data have been

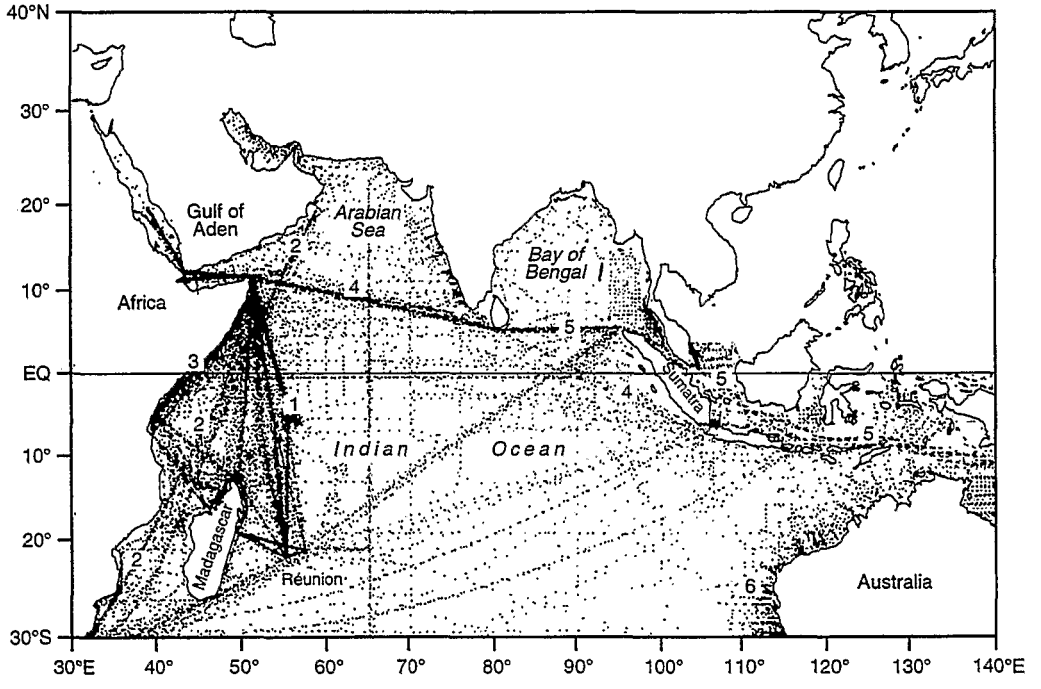

Fig. 1. Main tracks of the ships-of-opportunity in the tropical Indian Ocean.

carefully checked, and values we were doubtful about have been rejected, as well as SST more than 40°C or less than 8°C, and SSS more than 40 or less than 20.

The additional data came mainly from hydrographic stations and consist of 10,603 observations collected during the period 1965–1992. The data taken by ships-of-opportunity were not compared with the hydrographic measurements to investigate bias and accuracy. From the previous studies, the overall accuracy of the gridded surface fields is known to be better than 0.1 for SSS (Delcroix and Henin, 1991) and not better than 0.3°C for SST (Delcroix, 1993).

For the best sampled lines, the SSS and SST maximum and minimum, the standard deviation, and the location and months are presented in Table 2. The data on these tracks are binned by 1° latitude or longitude and averaged. The width of the tracks is generally less than 4–6°.

To facilitate the discussion the tracks were named as follows: Gulf of Aden–La Reunion (Track 1); Persian Gulf–Cape Town (Track 2); Gulf of Aden–eastern Africa (Track 3); Gulf of Aden–Indonesia (Track 4); Sri Lanka–Malacca Strait–Torres Strait (Track 5); west coast of Australia (Track 6).

Table 1. Locations of the different water-masses

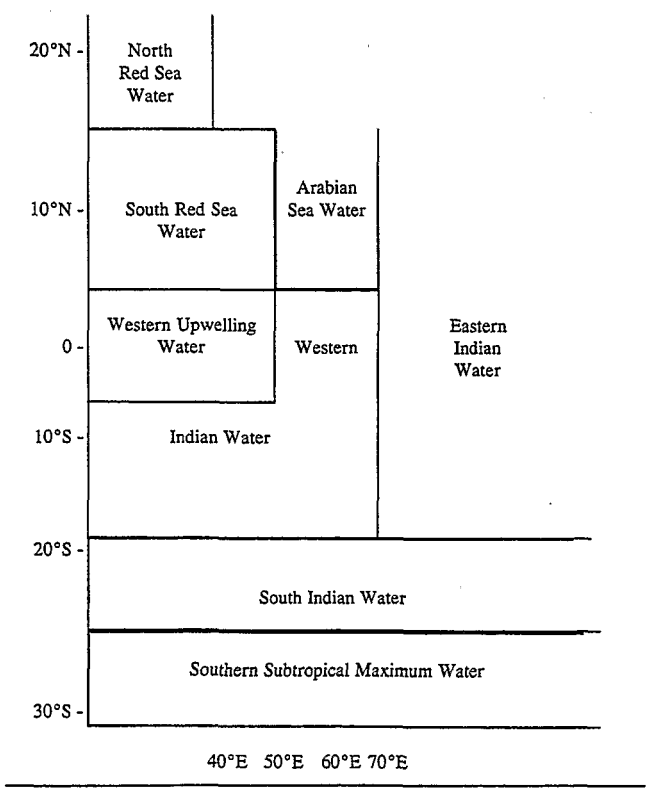

3 MEAN SEA-SURFACE OBSERVATIONS ALONG SHIPPING TRACKS

The western Indian Ocean, where data coverage is relatively good, is discussed first. Three tracks cross 10°N near the Horn of Africa (Fig. 1). Although the tracks are blurred in the figure, due to the different routes, Track 3 (Gulf of Aden–eastern Africa) is within a few miles of the coast, Track 1 (Gulf of Aden–La Reunion) is about 60 miles offshore, and Track 2 (Persian Gulf–Cape Town) is about 120 miles offshore, giving coverage on the scale of the upwelling zone in this region. The tracks then fan out into a large area extending southward to Madagascar.

3.1 *Track 1: Gulf of Aden–La Reunion* (12°N–22°S)

The track crosses the equator at 53°E (Fig. 1), well out of the upwelling zone. SST (Fig. 2) south of the equator presents a clear southern annual cycle with a maximum in February/March and a minimum in August. North of 5°S, the cycle is semiannual. The coldest water develops north of 8°N between July and September, averaging 24°C at 10°N (individual years may be lower), due to the upwelling at the Somalia coast. North of this area, in the Gulf of Aden, SST reaches its maximum (northern summer) and there is an intense temperature front at 12°N: in 1° of latitude, SST increases on average from 24 to 28°C. The second cool season, from November to February, is due to the combination of the northeast monsoon and the northern winter, and of course the front is not present at this time. It is much less intense than the previous one (temperature minimum 26°C at 11°N). The warmest water develops from March to May just before the onset of the Asian summer monsoon, when the temperature rises above 29°C. The second warm season, in October/November, is less intense with 27°C temperature.

The SSS cycle (Fig. 3) is also related to the monsoon, particularly north of the equator. North of 5°N, the salinity is always above 35.50, and north of 10°N it is above 36.00, with

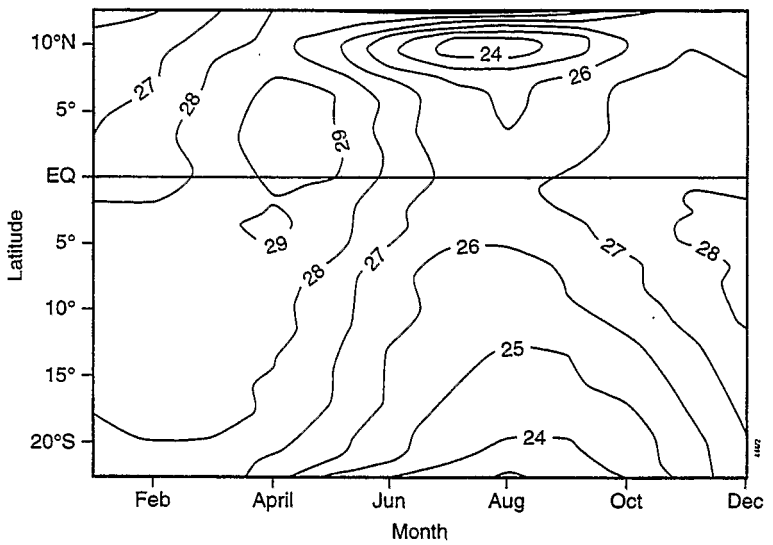

Fig. 2. Space–time diagram showing the mean annual cycle of SST along Track 1 (Gulf of Aden–La Reunion).

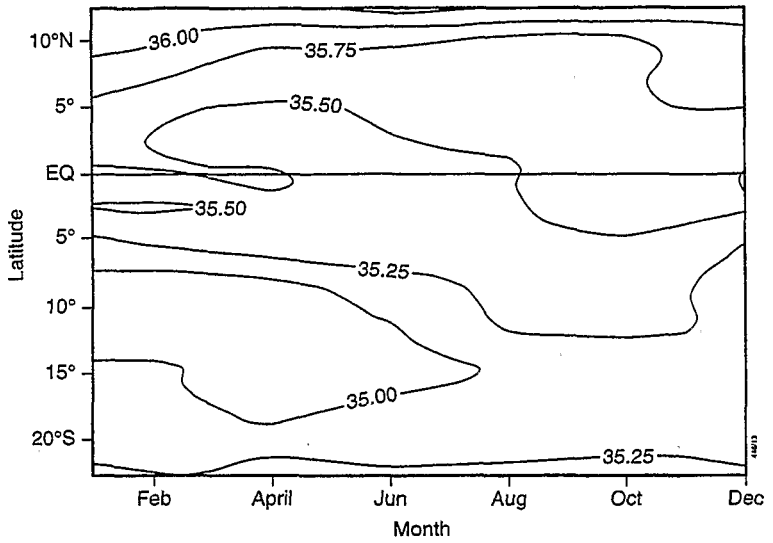

Fig. 3. Space–time diagram showing the mean annual cycle of SSS along Track 1 (Gulf of Aden–La Reunion).

little variation. During the southwest monsoon (from March to August), SSS increases in the region from the equator to 5°N, possibly due to upwelling and evaporation. South of the equator, SSS has a southern seasonal cycle. During the warm season, it is less than 35.00; during the cold season, it is over 35.00 from 20 to 10°S, increasing equatorward to 35.50. It seems obvious that the northern cycle of SSS is driven by the monsoon. Southwesterly wind in summer implies strong coastal upwelling, bringing to the surface water with salinity more than 35.5, which could eventually increase due to evaporation. The northeasterly wind in winter comes from the Asiatic continent and is very dry. It implies high SSS through evaporation and, due to the Ekman effect, this salty and cool water mass is driven southward along the African coast.

The southern SSS cycle is driven by austral seasonal variations. Low SSS during the first part of the year is due to the presence of the Intertropical Convergence Zone (ITCZ), centred at 10° S. In the second part of the year, the increase in SSS may in part be due to the evaporation by the strong winds of the summer monsoon, known to be a more intense season than the winter monsoon.

3.2 *Track 2: Persian Gulf–Cape Town* (20°N–30°S)

The track crosses the equator near 50°E and follows the Mozambique Channel (Fig. 1). The SST cycle between 10°N and 20°S has almost the same phase as along Track 1 (Fig. 4). The differences in temperature are small, with the notable exception that pools of 30°C water appear on Track 2, and the influence of coastal upwelling at 10°N is weaker because the track is further offshore. It seems obvious that the northern cycle of the SSS is driven by coastal upwelling bringing to the surface water with salinity more than 35.5, which could eventually increase due to evaporation. The northeasterly wind in winter comes from the Asiatic continent and is very dry. It implies high SSS through evaporation and, due to the Ekman effect, this salted and cool water mass is driven southward along the African coast.

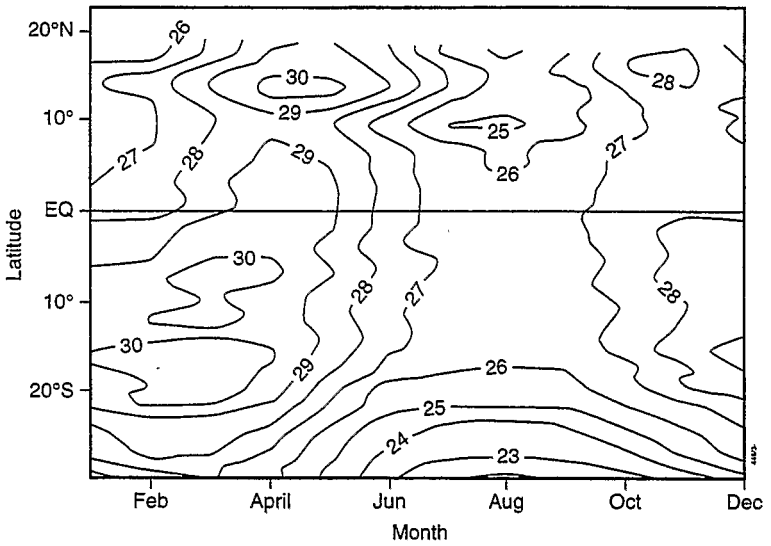

Fig. 4. Space–time diagram showing the mean annual cycle of SST along Track 2 (Persian Gulf–Cape Town).

South of 20°S and north of 10°N, other features appear, most notably a pool of 30°C north of the equator in April/May, before the onset of the Asian monsoon, and an upwelling at 20°N along the coast of Arabia. South of the equator, SST in the Mozambique Channel is 1°C higher than along Track 1 (Donguy and Piton, 1991), which suggests the channel is the warm pool of the southwestern Indian Ocean.

SSS between 20°S and 10°N (Fig. 5) is almost the same as along Track 1. North of 10°N, salinity is usually above 36.00 except during the Asian summer monsoon. South of 20°S, salinity is above 35.25.

3.3 *Track 3: Red Sea–Madagascar* (12°N–12°S)

The track runs along the east African coast, except in the southernmost part where it swings away from the coast and merges with Track 2, and in the north where it merges with Track 1 (Fig. 1). Consequently, SST and SSS patterns are close to the ones observed along Tracks 1 and 2 but with a stronger coastal influence, due to the proximity of the shore (sometimes only a few miles).

North of the equator (Fig. 6) the climate is cooler than along the two first tracks: in summer (May–October) due to the influence of the coastal upwelling, and in winter (November–February) due to advection close to the shore of cool water from the northeast monsoon. South of the equator, SST is similar to the pattern observed in the Mozambique Channel (Track 2) but cooler, mainly during the cold season (July–September).

The SSS cycle is also related to those of Tracks 1 and 2 (Fig. 7). In the northern hemisphere, SSS has a clear annual cycle connected to the monsoon. During the southwest monsoon, it increases from 35.25 at the equator to 36.25 at 11°N. During the northeast monsoon, it increases only from 35.50 at the equator to 35.75 at 11°N. These results support Donguy (1970), who used the same techniques in the same area for 1966–1967. The present SST and SSS climatologies (Figs 6 and 7) are in agreement with the schematic SST and SSS annual cycles defined in Figs 2 and 3 of Donguy (1970).

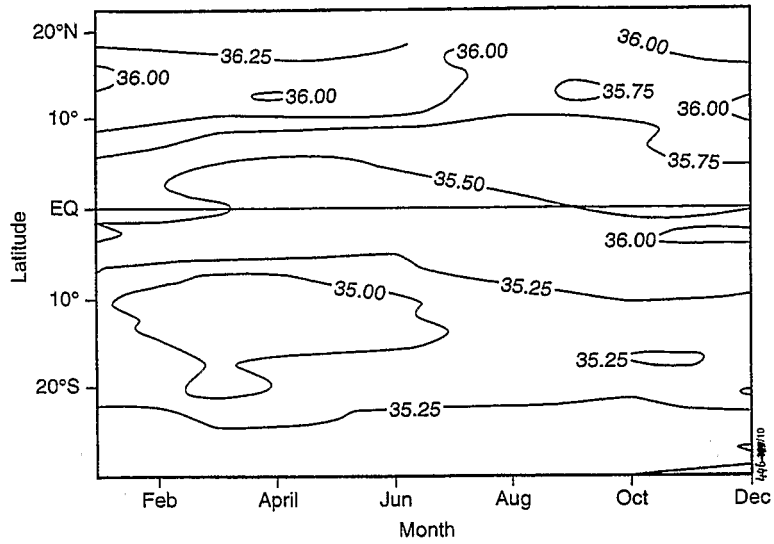

Fig. 5. Space–time diagram showing the mean annual cycle of SSS along Track 2 (Persian Gulf–Cape Town).

Moving away from the western Indian Ocean, the next two tracks show the zonal structure across the ocean and highlight the differences between east and west.

3.4 *Track 4: Djibouti–Java* (45°–105°E)

The track starts in the Gulf of Aden, crosses the Arabian Sea to south of Sri Lanka, then

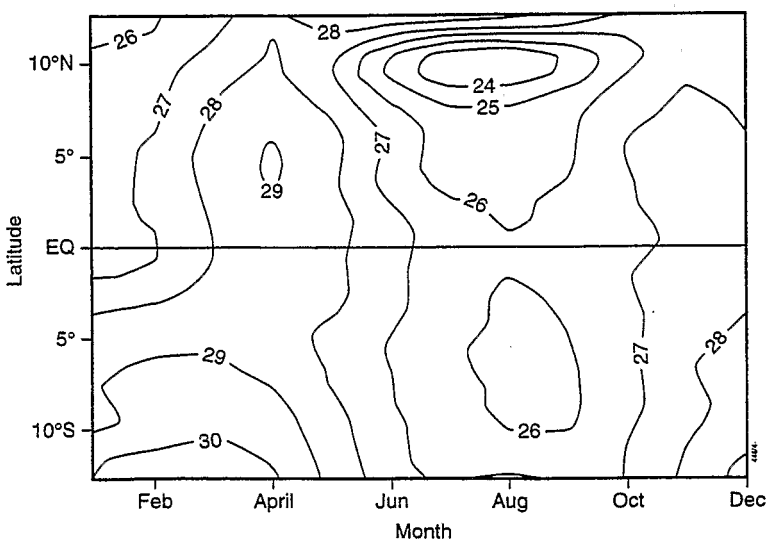

Fig. 6. Space–time diagram showing the mean annual cycle of SST along Track 3 (Gulf of Aden–eastern Africa).

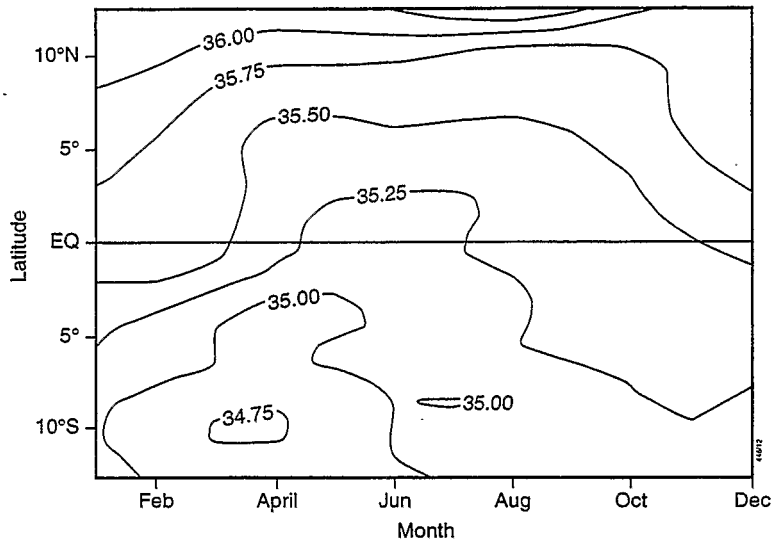

Fig. 7. Space–time diagram showing the mean annual cycle of SSS along Track 3 (Gulf of Aden–eastern Africa).

crosses the equator at about 90°E and reaches Java Island (Fig. 1). Along this track (Fig. 8), east of 60°E SST is usually more than 27°C, with much of the region having temperatures above 28°C throughout the year. West of 50°E, in the Gulf of Aden, the annual cycle is typically boreal. Slightly further to the east, the southwest monsoon induces coastal upwelling off the Horn of Africa from June to October with SST as low as 25°C. As in

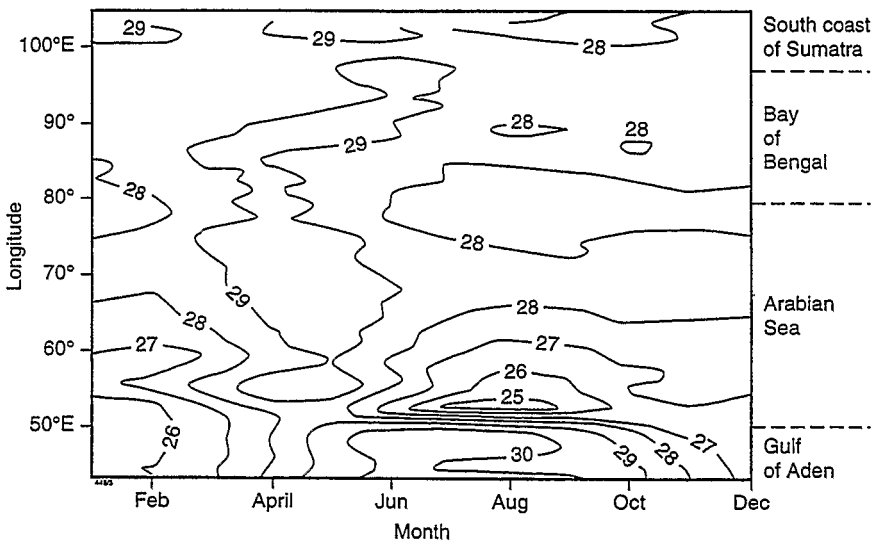

Fig. 8. Space–time diagram showing the mean annual cycle of SST along Track 4 (Gulf of Aden–Indonesia).

Track 1 (Fig. 2) an intense temperature front occurs at about 50°E. The upwelling influence appears to extend eastward to 65°E, implying advection of the upwelled water over a considerable distance while it maintains cool temperatures. Yet further to the east extending to 105°E, the warm season is from March to July with SST above 29°C, and the relatively cool season from June to October with SST about 28°C. In the Arabian Sea and in the Bay of Bengal, the warm season is due to the prevalence of light winds and the increase of heat content before the southwest monsoon, whereas the cold season is due to evaporation by the southwest monsoon itself. The thermal structure in the vicinity of the track (Sarma *et al.*, 1993) in the Arabian Sea confirms this analysis.

In SSS (Fig. 9), there are obviously two large-scale regimes along Track 4. West of 70°E, SSS is high, always above 35.00 and during the second part of the year above 36.00. In this regime, the 36.00 isohaline moves from 60°E in April to 70°E in October (i.e. 1000 km in 6 months), probably due to advection by monsoonal currents, with an inferred velocity of 6 cm/s. The SSS maximum occurs in August at 50°E and in October at 70°E. The second large-scale regime develops east of 80°E, where SSS is relatively low, always below 35.00. Between 70 and 90°E, in the vicinity of the Malabar Coast and Sri Lanka, SSS is less than 34.50 from October to June, probably due to the rainy season, but close to 35.00 the rest of the year. From 85 to 105°E, in the Bay of Bengal between Sri Lanka and Java, SSS is always less than 35.00, and east of 100°E close to the Sumatra coast, even less than 34.00. However, there is a westward extension of low SSS (less than 34.00) from 100 to 90°E from June to September, which is probably due to the ITCZ being south of the Bay of Bengal from April to June (Sadler *et al.*, 1987). A small-scale regime develops in the Gulf of Aden, west of 50°E, where the salinity maximum (above 36.50), which coincides with the temperature maximum, is due to strong and dry west winds inducing evaporation.

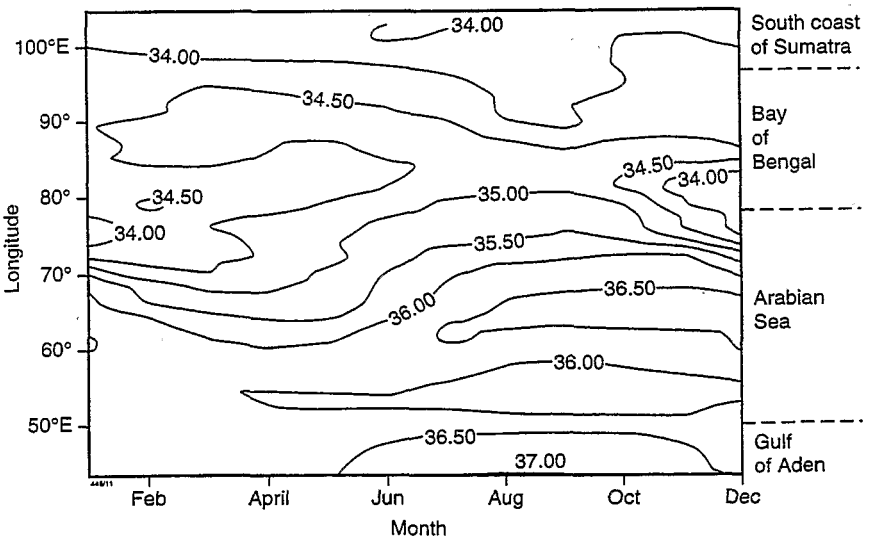

Fig. 9. Space–time diagram showing the mean annual cycle of SSS along Track 4 (Gulf of Aden–Indonesia).

3.5 *Track 5: Sri Lanka–Torres Strait* (80°–140°E)

The track runs from Sri Lanka, crosses the Bay of Bengal to the north end of Sumatra, follows the Malacca Strait crossing the equator at 105°E into the strait, then through the Java Sea and the Flores Sea until the Torres Strait. Subsequently, from 100 to 140°E, Track 5 follows internal waters.

In the Bay of Bengal, west of 95°E, the warm season (Fig. 10) is from March to June, with an SST maximum of 29°C, probably due to light winds and the presence of the ITCZ (Sadler *et al.*, 1987). During the cool season (southwest monsoon), SST is less than 28°C. There is no semiannual cycle as in the Arabian Sea. In the Malacca Strait (95°–105°E), SST is usually above 29°C, reaching 30°C in August/September. In the Java Sea (105°–115°E), SST is above 29°C in the warm season (April–August), when the east wind prevails, and below 28°C in the cooler season (November–March), when the west wind is blowing. Although the change in temperature in the Malacca Strait and Java Sea is small, they may impact climate due to the generally high temperatures. Conversely, in the Flores Sea seasonal contrasts are larger. During the warm season (November–May), SST is above 29°C. During the cool season (July–September), SST is less than 27°C, dropping to 26°C in August. The annual cycles in the Flores Sea and the Java Sea have a marked difference in phase, which may be related to the difference in water depth. The Java Sea is shallow, with depths about 50 m. In the Flores Sea, the water is deep and the east wind may induce coastal upwelling along the Celebes Islands. At the eastern end of this track, east of 130°E, SST is again less than 26°C from July to September and more than 29°C from November to May. The annual phase and amplitude of SST variation has a complex structure throughout the Indonesian archipelago, providing a real-world laboratory for studies of the surface heat budget. The differences in SST that develop are due to many mechanisms, including land–sea effects, cloud cover, evaporation, ocean circulation and stratification by salinity, making the development of a representative model a great challenge.

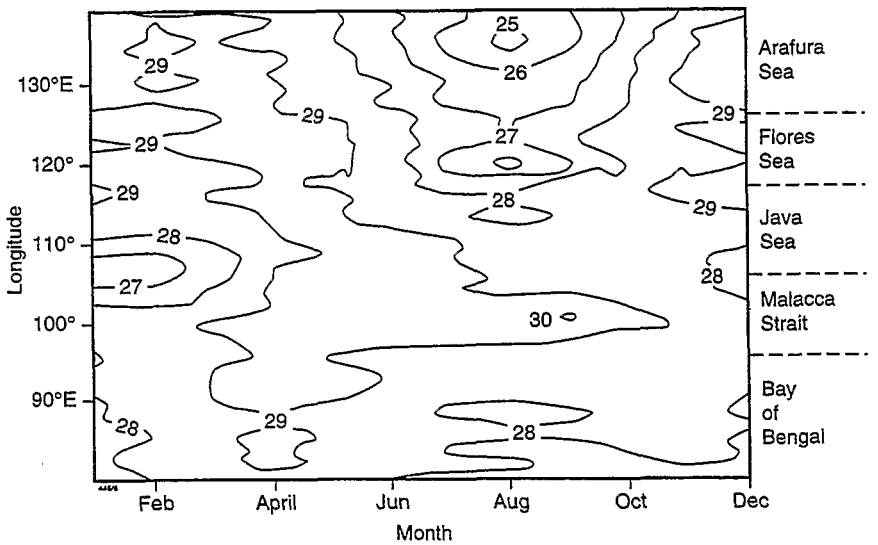

Fig. 10. Space–time diagram showing the mean annual cycle of SST along Track 5 (Sri Lanka–Malacca Strait–Torres Strait).

SSS along Track 5 (Fig. 11) is always less than 35.00, with only small seasonal contrasts. In the Bay of Bengal, west of 90°E, SSS is above 34.00 with the minimum in winter (November–February) and the maximum from July to October (dry season on the east coast of India). In Malacca Strait and the Java Sea, SSS is less than 34.00, with the minimum (32.00) in the cool season (November–March), which is the wettest season in Singapore. In the Flores Sea and the Arafura Sea a clear seasonal contrast appears: SSS is less than 34.00 from February to July and more than 34.00 from July to February. This seasonal cycle may be connected to the precipitation regime and to the wind. Precipitation on the northwest coast of Australia (not far from the Flores Sea) is highest in January and lowest in July. The SSS seems to respond with 2 months lag (Hires and Montgomery, 1972). Moreover, the cooling observed in the Flores Sea seems directly connected to the presence of SSS above 34.00, but in the Arafura Sea cooling and low salinity are concomitant. As the cooling is probably due to evaporation, this feature seems paradoxical. However, the cause of the unexpectedly low salinity could be run-off from New Guinea.

3.6 *Track 6: Along the southwest coast of Australia* (20°–35°S)

The track roughly follows the Leeuwin Current. However, south of 24°S, the Leeuwin Current is relatively narrow (less than 100 km), whereas the shipping route is 400 km wide. Consequently, this narrow current will not be the only strong influence on the regime of this area. SST is highest in April and lowest in September (Fig. 12), while SSS is lowest between April and September (Fig. 13) (in agreement with Cresswell and Golding, 1980). The regime is the same as the one prevailing in the triangular region north of Australia and south of Indonesia, where there is an accumulation of warm water from January to May and of cold water during the second part of the year. Moreover, SSS is low from March to August in the Arafura Sea (Fig. 11), which is the westernmost part of the triangle. Consequently, the

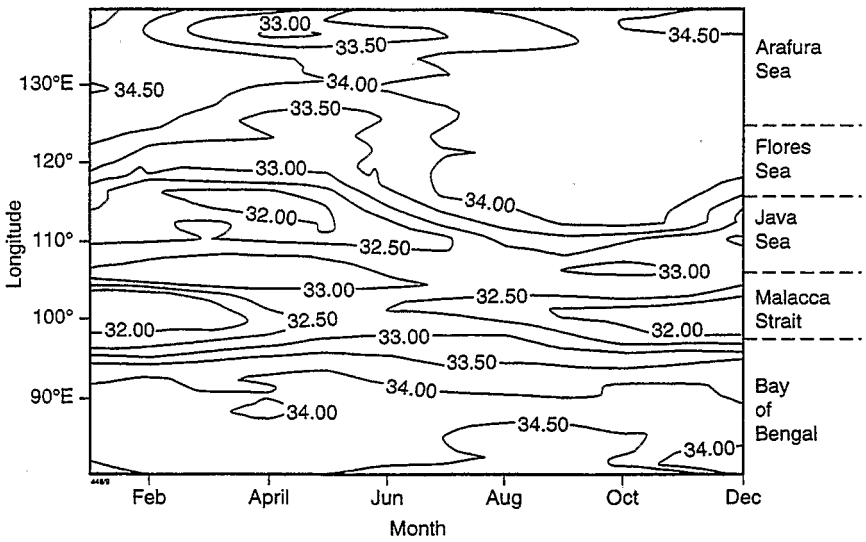

Fig. 11. Space–time diagram showing the mean annual cycle of SSS along Track 5 (Sri Lanka–Malacca Strait–Torres Strait).

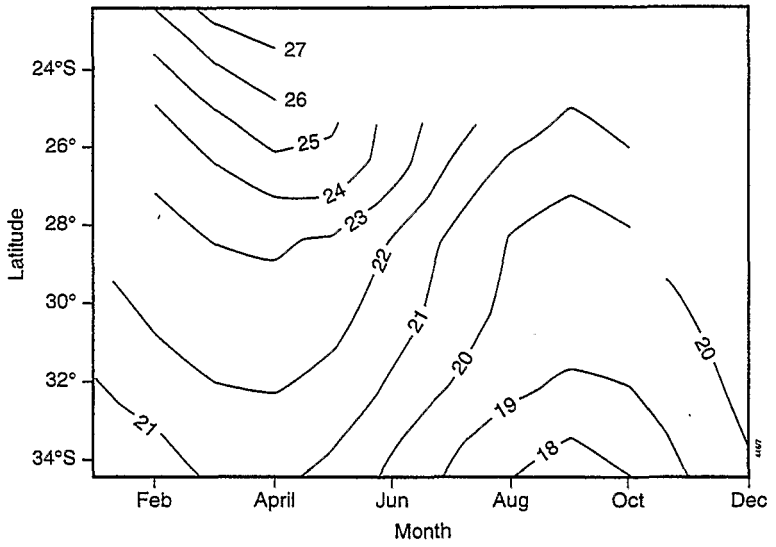

Fig. 12. Space–time diagram showing the mean annual cycle of SST along Track 6 (western coast of Australia).

waters along Track 6 seem to originate from the north and are at least partly carried south by the Leeuwin Current from March to September, as pointed out by Cresswell (1991). Moreover, at this time, the poleward sea-level gradient is at its steepest and is not counteracted by the equatorward wind stress, which is then very weak (Godfrey and Ridgway, 1985).

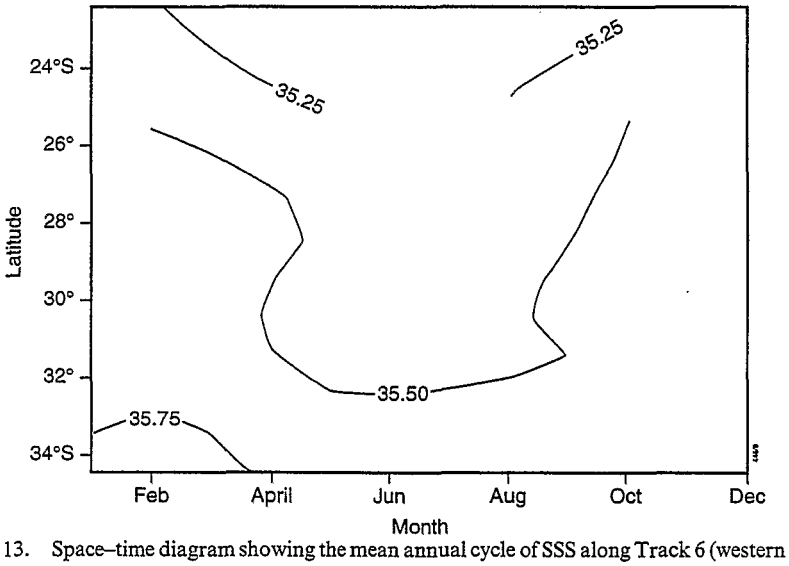

Fig. 13. Space–time diagram showing the mean annual cycle of SSS along Track 6 (western coast of Australia).

4 SURFACE WATER MASSES

Water masses are defined by salinity and temperature. The definition of the surface water masses for the entire tropical Indian Ocean is then possible from a T–S diagram (Donguy, 1970). The following classification is inferred from the surface T–S diagram for the data compiled for this study (Fig. 14).

$S > 38.0$	$T > 24.0°C$	North Red Sea Water
$36.5 < S < 38.0$	$T > 24.0°C$	South Red Sea Water
$36.0 < S < 37.0$	$18°C < T < 22.0°C$	Southern Subtropical Maximum Water
$35.5 < S < 36.5$	$T > 22.0°C$	Arabian Sea Water
$35.5 < S < 36.0$	$T < 22.0°C$	South Indian Water
$35.0 < S < 35.5$	$18.0°C < T < 24.0°C$	Western Upwelling Water
$34.5 < S < 35.5$	$T > 24.0°C$	Western Indian Water
$S < 34.5$	$T > 26.0°C$	Eastern Indian Water

Wyrtki (1971), with the data of the International Indian Ocean Expedition, has presented such a diagram from the surface to 25 m depth and the most important water masses may be recognised.

The geographic locations (Table 1) of these different water masses are as follows:

—Eastern Indian Water, east of 70°E, north of 20°S
—Western Indian Water, west of 70°E, north of 20°S, south of 10°N

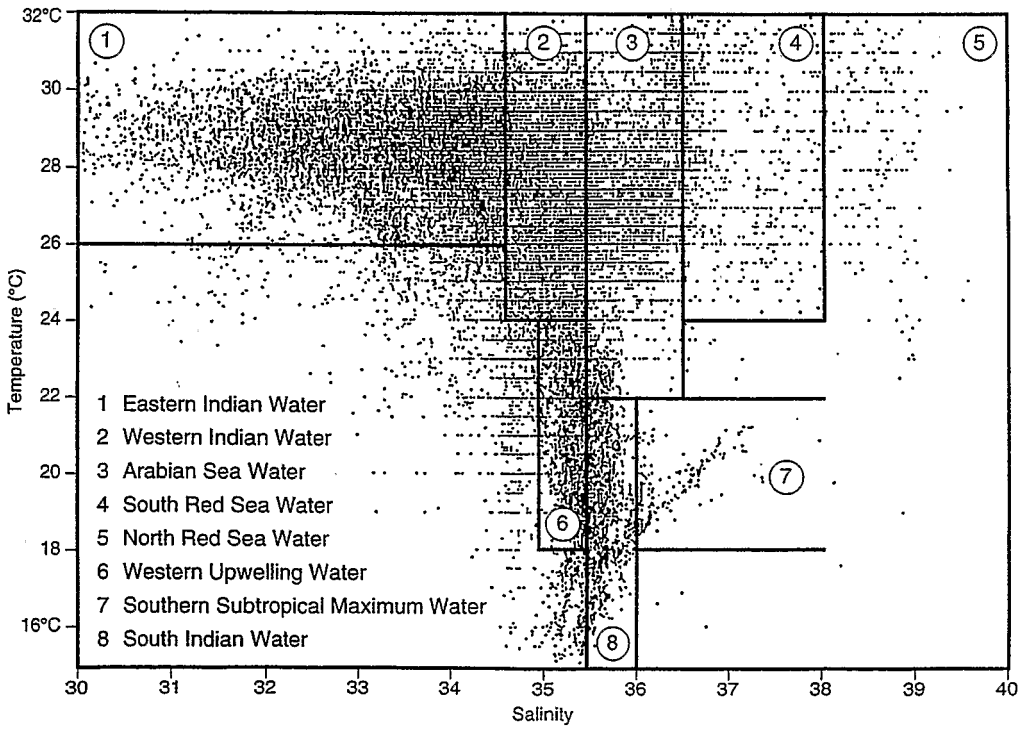

Fig. 14. T–S diagram from SST and SSS.

Table 2. Values of SSS and SST maximum and minimum, standard deviation, data number, location and month for each shipping track

	Max S	Min S	Max T	Min T
Line 1	36.49	34.23	29.99	22.52
σ	0.29	2.38	0.69	2.59
N. Data	36	14	11	30
Latitude	12.50°N	15.50°S	2.50°N	10.50°N
Longitude	53.03°E	54.58°E	53.58°E	53.14°E
Month	7	4	5	7
Line 2	36.44	34.47	31.33	23.51
			31.33	21.63
σ	0.09	0.78	1.15	2.94
			0.58	2.03
N. Data	4	3	3	7
			3	6
Latitude	17.50°N	20.50°S	13.50°N	17.50°N
			20.50°S	29.50°S
Longitude	58.30°E	39.66°E	56.34°E	58.30°E
			39.66°E	35.25°E
Month	5	3	5	7
			3	7
Line 3	36.51	34.56	30.75	21.44
σ	0.28	0.45	0.35	2.09
N. Data	10	5	2	18
Latitude	12.50°N	8.50°S	10.50°S	10.50°N
Longitude	52.78°E	41.50°E	42.17°E	51.89°E
Month	8	4	3	8
Line 4	37.26	33.14	31.32	23.02
σ	0.62	0.36	0.74	1.99
N. Data	19	3	24	5
Latitude	12.05°N	6.74°S	12.55°N	12.95°N
Longitude	43.50°E	104.50°E	48.50°E	52.50°E
Month	8	9	6	7
Line 5	35.52	30.46	30.23	23.73
σ	0.31	0.39	0.74	0.75
N. Data	2	22	16	3
Latitude	6.03°N	5.41°N	1.59°N	9.68°S
Longitude	80.50°E	100.50°E	106.50°E	136.50°E
Month	11	2	5	8
Line 6	35.87	34.18	30.67	16.89
σ	0.12	0.25	0.34	1.07
N. Data	15	5	5	24
Latitude	34.50°S	10.50°S	18.50°S	34.50°S
Longitude	114.88°E	129.25°E	117.25°E	114.88°E
Month	2	7	2	9

—Arabian Sea Water, west of 70°E, north of 10°N
—South Red Sea Water, west of 50°E, south of 15°N, north of 10°N
—North Red Sea Water, west of 40°E, north of 15°N
—Western Upwelling Water, west of 50°E, north of 5°S, south of 10°N
—South Indian Water, south of 20°S
—Southern Subtropical Maximum Water, south of 25°S

Each of the waters is formed by unique physical and climatological factors within its region. The salinity of the Southern Subtropical Maximum Water and South Indian Water has a small range, because these water masses are located in a dry area. Conversely, the salinity of the Eastern Indian Water has a large range (from 30 and even less to 34.5), because this water mass is located in a wet area characterized by the presence of the ITCZ. The North Red Sea Water is isolated inside the Red Sea, whereas the South Red Sea Water expands seasonally into the Gulf of Aden. West of 70°E, the expansion of the Western Indian Water and of the Arabian Sea Water is affected by monsoonal currents. The Western Upwelling Water appears only along the African coast during the southwest monsoon. Generally, the formation and location of these different water masses are due to the influence of winds, advection and the evaporation–precipitation balance.

5 BI-MONTHLY MEAN SSS AND SST CHARTS

Bi-monthly mean SSS and SST charts were drawn from all of the available data, approximately 6000 to 8000 observations for each 2-month period. The density of observations is variable, with some regions having very little or no data. There is a large amount of data in the western tropical Indian Ocean west of 60°E and in the Indonesian region, but the data are scarce in the southern Indian Ocean from 60°E to 110°E, with few individual ship tracks. As the seasonal signal is strong due to the monsoon phenomenon, the bi-monthly mean SSS charts are probably reliable (Fig. 15). The only previous charts are the bi-monthly SSS charts from Wyrtki (1971) and monthly SSS charts including only 1 year of observation in the western Indian Ocean by Donguy (1975). As there are already several sets of monthly SST charts (Wyrtki, 1971; Sadler *et al.*, 1987), our SST charts are not presented. The six SSS charts are presented in Fig. 15. Dots indicate where data are available and give an indication of the reliability of the charts.

The charts are described firstly in terms of the major features of SSS that develop during the peak monsoon seasons, which can be qualitatively associated with precipitation, evaporation or advection. Secondly, salinity is used as a tracer to estimate current speeds and the result compared to other measurements of currents.

During the Asian winter monsoon, from November/December to March/April (Fig. 15), the northeasterly winds in the northern hemisphere drive a westward current south of India. As a result, low-salinity waters are carried from the Bay of Bengal into the southern Arabian Sea. SSS less than 35.00 extends as far as 65°E in March/April. In the northern Arabian Sea, the surface water is cool and SSS is high due to evaporation by dry offshore winds ($35.5 < S < 36.5$, $T > 22.0$°C). This water is carried by coastal and Ekman currents southwestward along the east African coast. At the same time, low-salinity water ($S < 34.5$, $T > 26.0$°) identified as Eastern Indian Water, accumulates in the northeastern Bay of Bengal and feeds the low-salinity flow south of India. In the southern hemisphere the major feature of SSS is controlled by rainfall in the ITCZ near 10°S (Sadler *et al.*, 1987). By

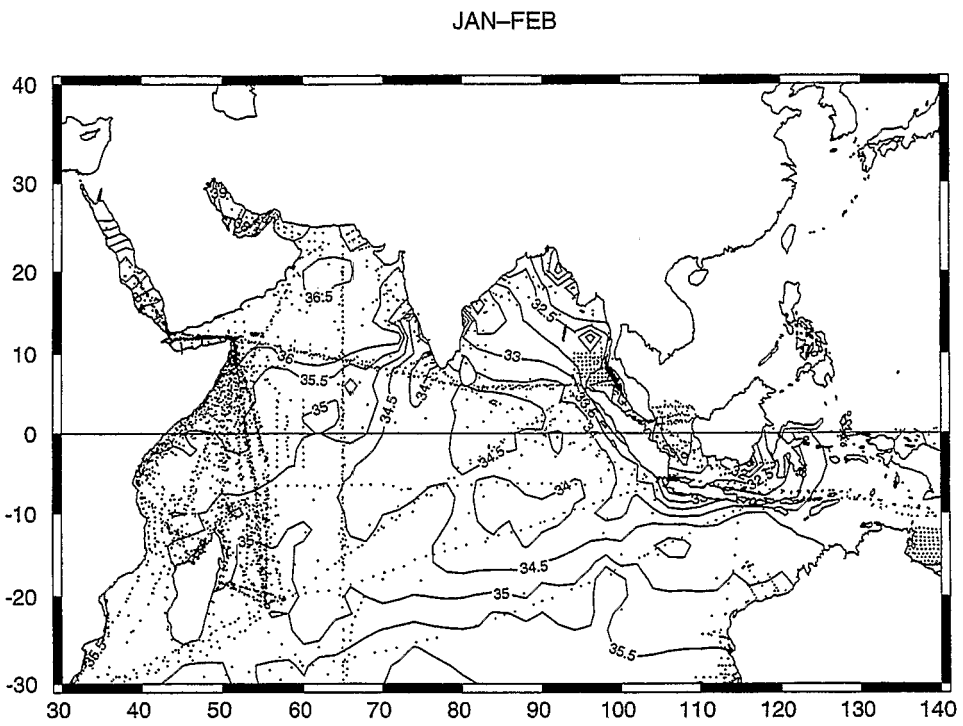

Fig. 15. Bi-monthly climatology of the SSS.

March/April a broad minimum of SSS extends from Indonesia to Madagascar, with SSS less than 34.5 reaching 70°E. South of the ITCZ, east of 100°E, high-salinity water is carried into the triangular region between Australia and Indonesia, probably by Ekman currents associated with nortwesterly winds.

During the Asian summer monsoon, from May/June to September/October (Fig. 15), the southwesterly winds north of the equator drive an eastward current south of India. The higher-salinity waters of the Arabian Sea are carried into the southern Bay of Bengal. The 35.00 contour moves back to 80°E during the season. The wind and currents are also reversed along the coast of Africa so that, in the western Indian Ocean, warm, low-salinity water identified as Western Indian Water ($34.5 < S < 35.5$, $T > 24.0$°C) is present in the Arabian Sea. This phenomenon has been abundantly documented (Knox, 1987). In the southern hemisphere, the easterly wind (trade wind) prevails pushing East Indian Water ($S < 34.5$, $T > 26.0$°C) westward from the Indonesian area and from the triangular region into the centre of the Indian Ocean (80°E).

In order to use SSS quantitatively as a tracer, we focus first on the Arabian Sea where, according to Donguy and Meyers (1995), an alternating gyre is centred at 5°N and 57°E. During the peak northeast monsoon (approximately November–February), the gyre is counterclockwise, whereas it is clockwise the rest of the time including the southwest monsoon. This movement appears on the SSS charts. Focusing on the area near 60°E, which is in the northwestward flowing part of the counterclockwise gyre during November–February, the 35.5 contour moves from 2°N in November/December to 8°N in January/February, implying a velocity of 12 cm/s. Similarly, during the season of a clockwise gyre,

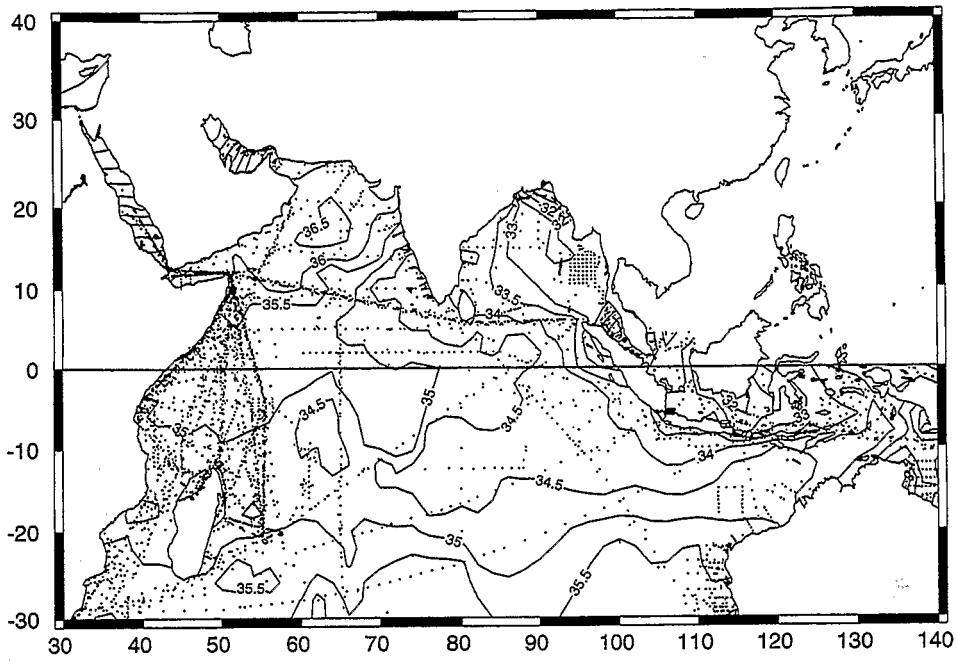

Fig. 15. (*Continued.*)

July to October, the 35.5 contour moves from 3°N to 3°S at 70°E, also with a velocity of 12 cm/s.

The second example of using SSS as a tracer is the semiannual equatorial jet. Focusing on the region between 68 and 76°E, the movement of the 35.0 contour in the vicinity of the equator from January/February to March/April gives an eastward velocity of 16 cm/s. Again, from July/August to March/April, movement of the contour suggests approximately the same speed eastward.

Two examples of using SSS as a tracer were chosen for the southern hemisphere. The effect of the South Equatorial Countercurrent (SEC) appears at 5°S with an eastward displacement of the 35.00 contour from 74 to 90°E during May/June to July/August, indicating a velocity of 32 cm/s. The effect of the SEC at 15°S appears as a westward movement of the 34.5 contour from 76°E in January/February to 70°E in March/April, implying a velocity of 12 cm/s.

When the speeds calculated from SSS contours are compared with currents measured by other methods, in all the cases the current velocity inferred from SSS features is smaller than that inferred from other measurements.

—The speed of the monsoonal gyre in the Arabian Sea estimated from SSS compares well to measurements during the northeast monsoon (Molinari *et al.*, 1990) but is too weak for the southwest monsoon. Wyrtki (1971) shows a geostrophic velocity of at least 40 cm/s from July to October.

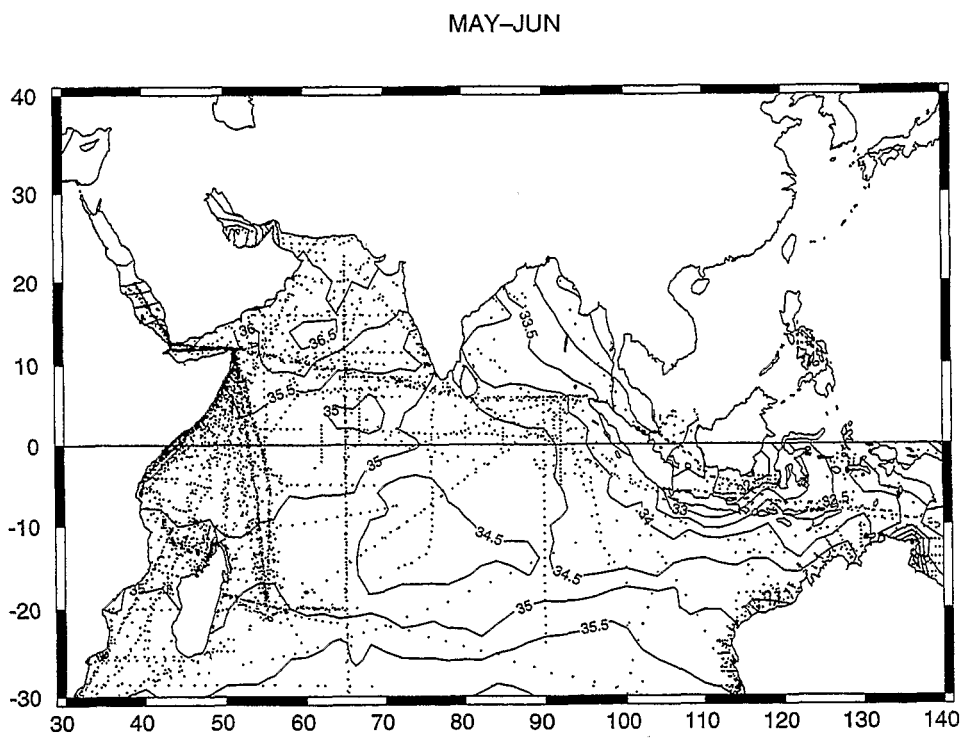

Fig. 15. (*Continued.*)

—The speed of the equatorial jet estimated from SSS is weak compared to the measurements of Wyrtki (1973), which suggest a speed greater than 43 cm/s. Molinari *et al.* (1990), from observations of drifting buoys, point out that, at the longitude considered, a speed of at least 50 cm/s would be expected. Reverdin (1987), after Cutler and Swallow (1984), shows that in May the velocity is more than 60 cm/s.
—The speed of the SEC estimated from SSS is about the same as observed values found by Molinari *et al.* (1990) and Wyrtki (1971).
—The speed of the SEC inferred from SSS is weak relative to measurements by Molinari *et al.* (1990) but about the same as measurements by Wyrtki (1971).

The discrepancies between the velocity from bi-monthly SSS used as a tracer and geostrophic calculations or direct measurements are not surprising. The SSS contours are not affected only by advection. However, the agreement in the direction of displacements gives us some confidence that details of the SSS fields are representative of real changes in the ocean.

6 COMPARISON WITH EARLIER STUDIES

Many papers provide considerations about near-surface variability in the Indian Ocean, but most of them investigate SST and there are few references to SSS. In addition to Wyrtki (1971), atlases present monthly variations of surface parameters: Sadler *et al.* (1987) from

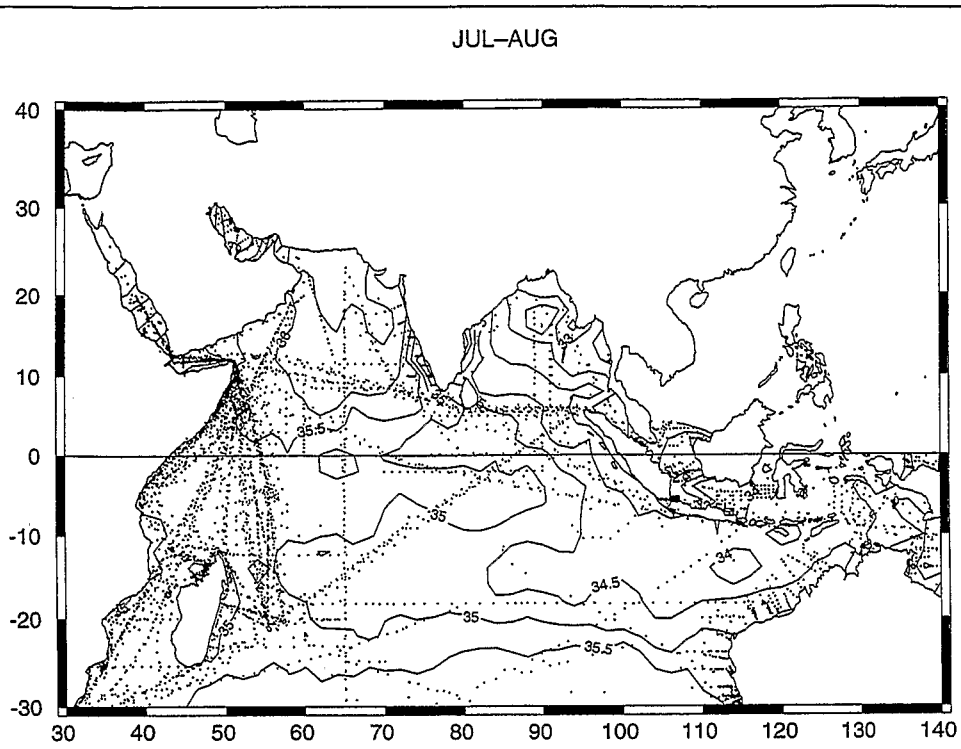

Fig. 15. (*Continued.*)

Cooperative Ocean–Atmosphere Data Set (COADS), Hastenrath and Lamb (1979) and Robinson *et al.* (1979). Few papers discuss surface climatology. Rao *et al.* (1989) with COADS data presents a climatology of the mixed-layer depth, SST and surface current. Reverdin (1987) compares a climatology issued from XBT data and SST to results from a model. McCreary and Kundu (1989) point out SST patterns from a numerical model. Owing to the monsoon phenomenon, the western Indian Ocean has attracted considerable attention: Molinari *et al.* (1986) for the 1979 FGGE, Reverdin and Fieux (1986) for the Sinode experiment and Bruce (1987) for the XBT observations from the tanker line Cape Town–Persian Gulf. Except for this last paper, there is no mention of SSS. In Robinson *et al.* (1979), monthly SST are very scarce north of 5°S. Moreover, there is only a yearly SSS map north of 5°S.

Space–time diagrams of SST have been drawn from Hastenrath and Lamb (1979) along three well-sampled lines (Track 1: Gulf of Aden–La Reunion, Track 4: Gulf of Aden–Indonesia, Track 5: Sri Lanka–Torres Strait). Between Gulf of Aden and La Reunion, the same features as in the present study appear: the same SST pattern with monsoon influence in the northern hemisphere and southern climate in the southern hemisphere. However, along the two other tracks, the present study shows much more detail and the SST is on average 1°C higher than in Hastenrath and Lamb (1979). Two SSS maps were also produced in this atlas: one corresponding to the northeast monsoon (November–April), the other corresponding to the southwest monsoon (May–October). The map featuring the southwest

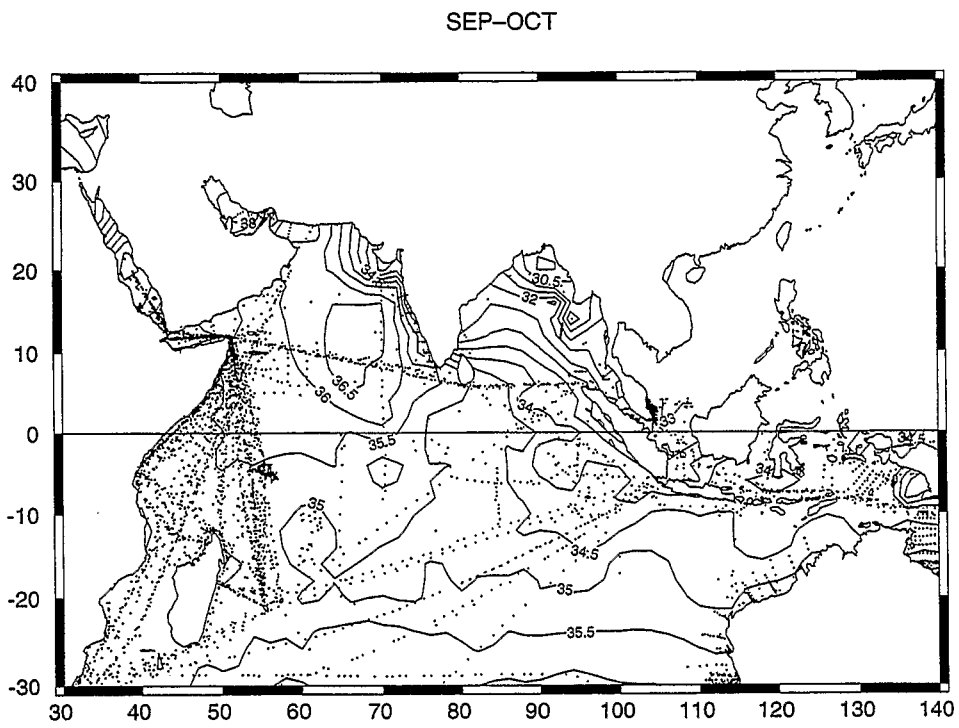

Fig. 15. (*Continued.*)

monsoon is similar to the July/August map from the present study; this is due to the robust characteristics and the long duration of the southwest monsoon. Conversely, the map featuring the northeast monsoon is different from the January/February map of the present study, but is rather similar to the November/December and March/April maps. This is due to the relative weakness of the northeast monsoon and its short duration. The true characteristics of the northeast monsoon featured in January/February are mixed with those of the monsoon transition (November/December and March/April).

From 1975 through July 1979, XBT and surface sampling were obtained along the Persian Gulf–Cape Town track corresponding to the present Track 2. Fifty-five transects including SST and SSS are available (Bruce, 1981, 1987). Space–time diagrams may be compared to Figs 4 and 5, but these figures represent a standard year and Bruce (1981, 1987) shows individual years. These latter might instead be compared to those issued from an earlier experiment (Donguy, 1970) in 1966–1967. Although the data are more scarce between 1975 and 1979 than in 1966–1967, the temperature diagrams are very similar, showing regular seasonal variations connected to the monsoon. The salinity diagram from Bruce (1981) also shows clear seasonal variations but limited at 2°S, comparable to Fig. 5 of the present study and to Fig. 7 from Donguy (1970). However, it seems that the SSS values from Bruce (1981) are greater than in both studies.

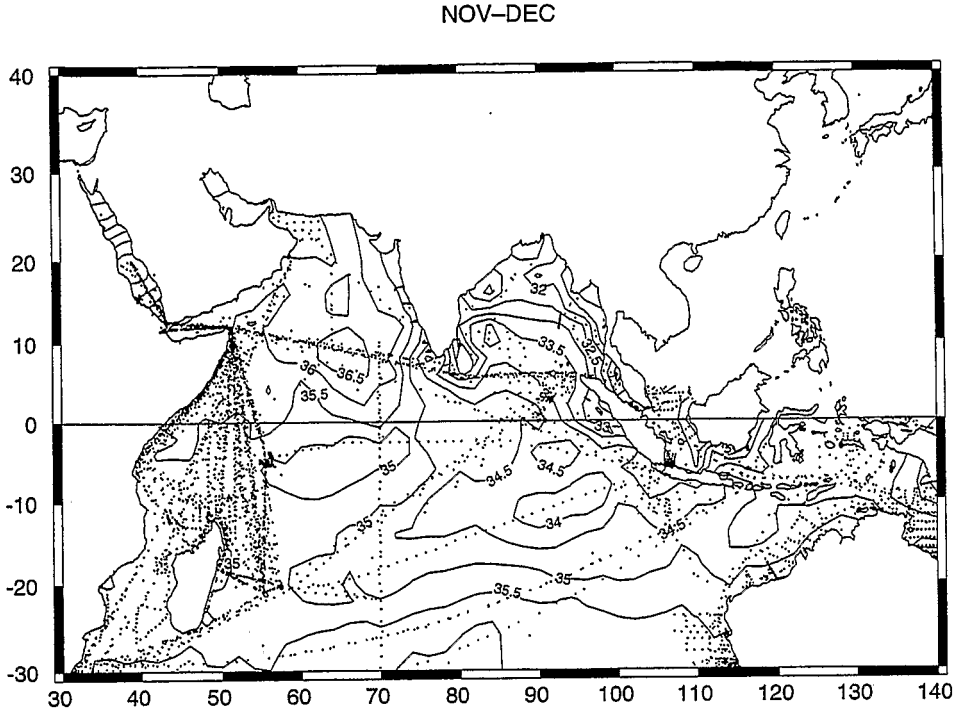

Fig. 15. (*Continued.*)

7 CONCLUSION

From the ORSTOM–CSIRO surface data set collected from 1965 to 1992, supplemented by all the available additional surface data, it was possible to draw a climatology of SST and SSS in the tropical Indian Ocean. Unfortunately, data are scarce in the centre of the ocean and are collected slowly by the present observational programme. After several years of new observations, strengthened by the use of themosalinographs, it is hoped that it will be possible to study interannual variations and, for example, the impact of ENSO on the surface properties of the tropical Indian Ocean.

Acknowledgements—Volunteer observers on merchant ships have generously collected the data in the field. Michel Prive was in charge of ORSTOM observations in Le Havre (France). L. Pigot of CSIRO processed the data. We gratefully acknowledge all this support.

REFERENCES

Bruce J. G. (1981) Variations in the Thermal Structure and Wind Field Occurring in the Western Indian Ocean during the Monsoons. Technical Report 272, Naval Oceanographic Office, 171 pp.

Bruce J. G. (1987) Seasonal heat content variations in the northwestern Indian Ocean. *Oceanologica Acta.* Proceedings International Symposium on Equatorial Vertical Motion Paris, 6–10 May 1985, pp. 77–83.

Cresswell G. R. (1991) The Leeuwin Current. Observations and recent models. *Journal of the Royal Society of Western Australia*, **74**, 1–14.

Cresswell G. R. and J. J. Golding (1980) Observations of a south-flowing current in the southeastern Indian Ocean. *Deep-Sea Research*, **27**, 449–466.

Cutler A. and J. Swallow (1984) Surface currents of the Indian Ocean (to 25°S, 100°E) compiled from historical data archived by the Meteorological Office, Bracknell, U.K. Report No. 187, Institute of Oceanographic Sciences, Surrey, U.K., 8 pp.

Delcroix T. (1993) Seasonal and interannual variability of sea-surface temperature in the tropical Pacific, 1969–1991. *Deep-Sea Research I*, **40**, 2217–2228.

Delcroix T. and C. Henin (1989) Mechanisms of subsurface thermal structures and sea surface thermohaline variabilities in the southwestern tropical Pacific during 1975–1985. *Journal of Marine Research*, **47**, 777–812.

Delcroix T. and C. Henin (1991) Seasonal and interannual variations of sea surface salinity in the Tropical Pacific Ocean. *Journal of Geophysical Research*, **96**, 22135–22150.

Dessier A. and J. R. Donguy (1994) The sea surface salinity in the tropical Atlantic between 10°S and 30°N. Seasonal and interannual variations (1977–1989). *Deep-Sea Research I*, **40**, 81–100.

Donguy J. R. (1970) Observations de surface le long des lignes de navigation dans la partie Ouest de l'Océan Indien. *Cahiers Océanographiques*, **224**, 353–366.

Donguy J. R. (1974) Une année d'observations de surface dans la zone de mousson de la partie occidentale de l'Océan Indien. *Cahiers ORSTOM Ser. Océanographie*, **122**, 117–128.

Donguy J. R. (1975) Les eaux superficielles tropicales de la partie occidentale de l'Océan Indien en 1966–1967. *Cahiers ORSTOM ser. Océanographie*, **131**, 31–47.

Donguy J. R. and G. Meyers (1995) Observations of geostrophic transport variability in the Western Tropical Indian Ocean. *Deep-Sea Research I*, **42**, 1007–1028.

Donguy J. R. and B. Piton (1991) The Mozambique Channel revisited. *Oceanologica Acta*, **14**, 6.

Godfrey J. S. and K. R. Ridgway (1985) The large-scale environment of the poleward-flowing Leeuwin Current, Western Australia: longshore steric height gradients, wind stresses and geostrophic flow. *Journal of Physical Oceanography*, **155**, 481–495.

Hastenrath S. and P. Lamb (1979) *Climatic atlas of the Indian Ocean* Part 1: *Surface circulation and climate*. University of Wisconsin Press, WI, 104 pp.

Hires R. J. and R. B. Montgomery (1972) Navifacial temperature and salinity along the track from Samoa to Hawaii, 1957–1965. *Journal of Marine Research*, **30**, 177–200.

Knox R. A. (1987) The Indian Ocean: interaction with the monsoon. In: *Monsoons*, J. S. Fein and P. L. Stephens, editors, John Wiley, New York, pp. 365–397.

Lukas R. (1989) Freshwater input on the Western Equatorial Ocean and air–sea interaction. In: *Proceedings of the symposium on western tropical Pacific air–sea interactions, Beijing, China*, 15–17 November 1988.

McCreary J. P. and P. K. Kundu (1989) A numerical investigation of sea surface temperature variability in the Arabian Sea. *Journal of Geophysical Research*, **94**, 16097–16114.

Molinari R. L., J. Swallow and J. F. Festa (1986) Evolution of the near-surface thermal structure in the western Indian Ocean during FGGE, 1979. *Journal of Marine Research*, **44**, 739–762.

Molinari R. L., D. Olson and G. Reverdin (1990) Surface current distributions in the tropical Indian Ocean derived from compilations of surface buoy trajectories. *Journal of Geophysical Research*, **97**, 20169–20178.

Rao R. R., R. L. Molinari and J. F. Festa (1989) Evolution of the climatological near-surface thermal structure of the tropical Indian Ocean. 1 Description of mean monthly mixed-layer depth and sea surface temperature, surface current and surface meteorological fields. *Journal of Geophysical Research*, **94**, 10801–10815.

Reverdin G. (1987) The upper equatorial Indian Ocean: the climatological seasonal cycle. *Journal of Physical Oceanography*, **17**, 903–927.

Reverdin G. and M. Fieux (1986) Sections in the western Indian Ocean. Variability in the temperature structure. *Deep-Sea Research*, **34**, 601–636.

Robinson M., R. Bauer and E. Schroeder (1979) Atlas of North Atlantic–Indian Ocean monthly mean temperatures and salinities of the surface layer, Ref. Publ. 18. Naval Oceanographic Office.

Sadler J. C., M. A. Lander, A. M. Huri and L. K. Oda (1987) *Tropical marine climatic atlas*. Vol. 1. *Indian and Atlantic Ocean*. NOAA, Department of Meteorology, University of Hawaii.

Sarma Y. V., S. S. Sarma and L. V. Gangadhara Rao (1993) Thermal structure of the Western Indian Ocean during the Southwest monsoon, 1983. *Oceanologica Acta*, **161**, 45–52.

Wyrtki K. (1971) *Oceanographic atlas of the International Indian Ocean Expedition*, National Science Foundation, Washington DC, 531 pp.

Wyrtki K. (1973) An equatorial jet in the Indian Ocean. *Science*, **181**, 262–264.